Dynamic Stability of a Helicopter with an External Suspended Load

Giorgio Guglieri*
Associate Professor

Paolo Marguerettaz
Ph.D. Student

Dipartimento di Ingegneria Meccanica e Aerospaziale
Politecnico di Torino, Torino, Italy

A simplified but comprehensive model for helicopter and external suspended load, based on the linear superposition of effects, is defined. The coherence of the external load modal response and of the helicopter response to control input is verified through available reference data. Finally, the impact of the slung load on the overall system dynamic stability, on the helicopter response to control input, and on flight qualities is assessed.

Nomenclature

A	cable cross section, m^2
$[A]$	state space helicopter matrix
a	acceleration, m/s^2
C_D	drag coefficient
C_L	lift coefficient
C_M	pitching moment coefficient
C_N	yawing moment coefficient
C_S	side-force coefficient
D	drag forces vector, N
DOF	degrees of freedom
F	force vector, N
f	residual
g	gravity acceleration, m/s^2
i, j, k	unit vectors along x, y, z axis
J_x, J_y, J_z, J_{xz}	moments of inertia, $kg \cdot m^2$
K	suspension line elastic constant, N/m
K_G	gravity forces vector, N
L	suspension line length, m
$[L_{BE}]$	rotation matrix from body to inertial axes
M, N	moments w.r.t. y and z axes, Nm
m	mass, kg
p, q, r	angular speed w.r.t. x, y, and z axes, rad/s
R	position vector, m
S	reference area, m^2
u, v, w	velocity components along x, y, and z axes, m/s
V	velocity vector, m/s
X, Y, Z	forces along x, y, and z axes, N
$[X]$	states vector
ΔL	elongation vector (cable)
ρ	air density, kg/m^3
ζ	damping coefficient, kg/s
φ, ϑ, ψ	Euler angles, rad
Ω	angular velocities vector, rad/s

Superscripts and subscript

A	aerodynamic
B	body frame
C	cable
CG	center of mass
E	ground fixed inertial frame
eff	effective
el	elastic
F	fuselage
FW	far wake
H	helicopter
L	load
LS	suspension point (load)
MR	main rotor
ref	reference
sp	suspension point
W	wake
x, y, z	x, y, z axes
ζ	damping

Introduction

Carrying external suspended loads is a typical helicopter mission. Both military and commercial operators widely exploit the capabilities of helicopters to rapidly move heavy and bulky loads in remote locations. Logging, construction, fire-fighting, search and rescue, and tactical transportation are only some of the possible missions in which a helicopter

*Corresponding author; email: giorgio.guglieri@polito.it.
Manuscript received September 2012; accepted April 2014.

carries a suspended load. Unfortunately, a suspended load adds its aerodynamics, rigid body dynamics, and elastic suspension dynamics to that of the bare airframe helicopter. Less than satisfactory handling can result from the combined systems, and the flight envelope can be restricted significantly because of operational safety concerns. Actually, external suspended load operations account for more than 10% of helicopter accidents, often with severe consequences (Ref. 1). A careful study of helicopter dynamics and the assessment of flight and handling qualities are therefore vital for safe operations.

Helicopter dynamics with an externally suspended load have been widely investigated since the extensive use of helicopters in the Vietnam War in the 1960s and 1970s. Early studies focused mainly on hover or low-speed flight dealing with reduced order helicopter models, modeling the slung load as a pendulum and neglecting aerodynamics effects (Ref. 2). Results showed a stable pendulum mode, but, in some combination of load weight and cable length, helicopter instability could arise. Further work investigated precision hover with a slung load and verified that conventional stability augmentation systems were not up to the task; thus different possible stabilization techniques were studied. Better results were obtained by feeding back relative motion of the load and helicopter to cyclic pitch (Ref. 3). A theoretically good alternative stabilization scheme required the active displacement of the suspension point (Ref. 4). A practical implementation was explored in Ref. 5. The external load was not connected directly to the helicopter; instead, the suspension lines were attached to two hydraulically actuated and electronically controlled movable arms. The system was flight-tested successfully, proving able to greatly increase the damping ratio of the load pendulum modes. Flight test also demonstrated that this approach made possible Instrument Flight Rules operations with suspended loads. In addition to electronic stabilization, appropriate piloting techniques were also investigated for various maneuvers (Ref. 6). More recent studies address stability with more complex models. Reference 7 develops a stability analysis based on a state space helicopter model decoupled in the longitudinal and lateral-directional planes. The load is modeled as a pendulum affected by isotropic drag and suspended by an inelastic cable. Results showed stability dependency on both cable length and load weight with the possibility of mildly unstable modes with increasing weight and cable length. In Ref. 8, full nonlinear rigid body equations for helicopter dynamics and rotor flap dynamics were derived and then linearized for a stability study. Cable length, position of the suspension point with respect to the helicopter center of mass, and load weight all affected stability. Depending on the combination of parameters, some modes could experience weak instability.

Most of the previously described studies neglected the aerodynamics of the load because they were focused on hover or low-speed flight. Slung loads usually are bluff bodies and may experience instability due to unsteady flows. Studies conducted on containers and cylindrically shaped loads in forward flight showed that increasing cable length, load weight, and speed improved stability (Ref. 9). These results were only partially confirmed by other works that pointed out that longer cables were destabilizing, but discrepancies can be an effect of the different aerodynamics of the load (Ref. 10). Despite the fact that most works try to address specific cases, it is generally possible to say that high drag proves to be destabilizing and lateral-directional motions are more affected by load dynamics than longitudinal ones. This is confirmed in Refs. 11 and 13, where extensive flight test and frequency responses obtained by system identification show that increasing load weight reduces lateral bandwidth, whereas the longitudinal one is much less affected. Reference 12 analyzes helicopter dynamics with a suspended load in forward and turning flight. The proposed helicopter model is fully nonlinear, includes single blades flapping/lagging and rotor inflow and has been validated with flight-test data (Ref. 14). The load is modeled as a pendulum affected by isotropic drag and suspended by an inelastic cable. Results show that pendulum modes can easily couple with helicopter Dutch roll leading to a degradation of flying qualities, whereas effects on longitudinal motions are much less relevant. Unsteady aerodynamic behavior of specific loads, in particular containers, has been widely investigated with simulation, wind tunnel testing, and flight test (Refs. 15, 16). It is known that external load instability can reduce the safe flight envelope well below limits due to power loading. Reference 17 provides means to passively stabilize a container, effectively restoring a useful flight envelope up to power limits.

Many studies have focused on external load modeling. In particular, Ref. 18 describes in detail a formulation valid for an arbitrary number of loads, suspensions lines, and even helicopters. Reference 19 proposes an interesting formulation to describe a generic slung load system taking into account different suspension combinations and cable collapse and tightening.

Helicopter handling qualities are widely addressed in Ref. 20. Reference 21 proposes qualitative and quantitative handling qualities criteria that specifically apply to suspended load operations. In particular, degraded visual environment (DVE) operations with loads up to one third of the helicopter mass are investigated, because, due to experience, they are considered the most demanding configurations. The quantitative criterion prescribes a lower limit in the available longitudinal and lateral-directional bandwidths. If the bandwidth is greater than the limit, and the helicopter without external load is rated as Level 1 on the Cooper–Harper scale when performing a specific maneuver, then a Level 1 rating is also assured when performing that maneuver with an external load. Reference 21 clearly states that "Not meeting this [bandwidth] criteria will result in handling qualities that are no worse than Level 2 with an externally slung load in the DVE, as long as the load-off handling qualities are Level 1. There is no Level 2-3 limit that is specifically due to external load."

Present Work

The objective of this work is the integration of a simplified but comprehensive helicopter model combined with two representations of the external suspended load (i.e., pendulum and six-degree-of-freedom (DOF) load models). This approach may be of interest for parametric design analysis and during the preliminary design phases when accurate simulation models are still unavailable. The coherence of external load modal dynamics and the helicopter response to control input is then verified with available reference data. Finally, the impact of slung load parameters on helicopter dynamic stability (eigenstructure), response to control input, and handling qualities are assessed.

Mathematical Model

As shown in Ref. 23, in the case of articulated rotor helicopters, reduced order models can be used to obtain a comprehensive approximation of short-term longitudinal, lateral directional, and heave dynamics when the complete system is weakly coupled. Results presented in Ref. 23 were not in themselves restricted to a small interval of time showing that it is also possible to perform a limited time domain simulation. In any case, when the reduced order model is derived from a higher order representation, it always assumes that the transformation is obtained performing a successful partitioning of states. The dynamic system composed of helicopter and external suspended load can be considered as weakly coupled. Reference 12 demonstrates that higher order dynamics, such as rotor and inflow dynamics, have a modest effect on the stability of the lowest frequency modes of the aircraft and the load (frequency and damping of the

Table 1. Helicopter main characteristics

Characteristic	Value
Weight (kg)	6800
Main rotor radius (m)	8.2
Main rotor speed (rad/s)	27
Blade number	4

phugoid, Dutch roll, and load modes do not change by more than about 5% when rotor and inflow dynamics are taken into account). Hence, a quasi-steady rotor model (i.e., incorporating the fuselage states and the suspended load dynamic model) is probably sufficiently accurate to represent the modal response of the vehicle–load system. Furthermore, this approach may balance the level of modeling complexity for the helicopter and the slung load.

Helicopter model

In this study, the helicopter representation is a state space model with nine states. A medium lift tactical utility helicopter with an articulated rotor is considered. The state space model derives from the full-state linearization and condensation to fuselage states of the nonlinear rigid blade model used in Ref. 12. The main helicopter characteristics are reported in Table 1.

State space matrices are obtained in trimmed conditions for different load and forward flight speed. In the solution process, helicopter state space matrix coefficients are used to reconstruct the nine equations of motion, evaluating linear and angular velocities and attitude angles in body axes. The state vector is

$$[X_H] = [u_H, v_H, w_H, p_H, q_H, r_H, \varphi_H, \vartheta_H, \psi_H]^T \tag{1}$$

The system is defined as

$$[\dot{X}_H] = [A]X_H + [B]u_H \tag{2}$$

where $\dot{X}_H$ is the derived states vector, A the state space matrix, B the control matrix, and u_H the controls vector. Three additional equations account for helicopter center of mass position in an inertial frame. These are, in matrix form,

$$[V_{\mathrm{HE}}] = [\dot{x}_{\mathrm{HE}}, \dot{y}_{\mathrm{HE}}, \dot{z}_{\mathrm{HE}}]^T = \left[L_{\mathrm{BE}_H}\right][u_{\mathrm{HB}}, v_{\mathrm{HB}}, w_{\mathrm{HB}}]^T \tag{3}$$

where L_{BE} is the rotation matrix from body axes to a ground fixed frame.

External load as a pendulum

Two approaches have been used to model the external load. In both cases, one suspension line only is connected to one point on the helicopter and one on the load. In the first case, the load is modeled as a spherical pendulum with the mass supposed to be a point mass. The only aerodynamic force acting on the pendulum is an isotropic drag. Since the focus of the analysis is on low speed and the suspension line has a negligible weight with respect to the load, the cable is modeled as inextensible, weightless and does not contribute to drag (Ref. 12).

System geometry is given in Fig. 1. The body reference frame (subscript B) originates in the helicopter center of gravity, the X axis is along the fuselage longitudinal axis and positive in the forward direction, the Z axis lies in the fuselage symmetry plane and points downward, the Y axis is oriented in the way the reference frame is right-handed. The Hook reference frame (subscript SP) is defined as thebody frame but it originates at the suspension point.

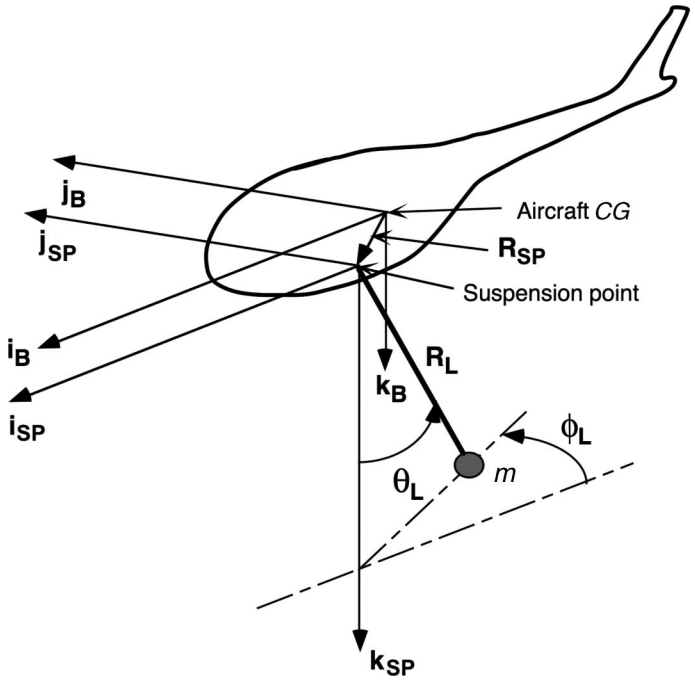

Fig. 1. System geometry.

Load position is described by φ_L, the azimuth angle, and by ϑ_L, the angle between the cable and the Z axis. The position vector $\vec{R}_L$ with respect to the suspension point is defined as

$$\vec{R}_L = -L\sin\theta_L\cos\varphi_L\vec{i}_{\mathrm{SP}} + L\sin\theta_L\sin\varphi_L\vec{j}_{\mathrm{SP}} + L\cos\theta_L\vec{k}_{\mathrm{SP}} \tag{4}$$

The position of the suspension point $\vec{R}_H$ with respect to the center of gravity of the helicopter is

$$\vec{R}_{\mathrm{SP}} = x_{\mathrm{SP}}\vec{i}_{\mathrm{SP}} + y_{\mathrm{SP}}\vec{j}_{\mathrm{SP}} + z_{\mathrm{SP}}\vec{k}_{\mathrm{SP}} \tag{5}$$

The absolute velocity $\vec{V}_L$ of the load is

$$\vec{V}_L = \vec{V}_{CG} + \dot{R} + \vec{\Omega}\times\vec{R} \tag{6}$$

where $\vec{R} = \vec{R}_{\mathrm{SP}} + \vec{R}_L$ is the position vector of the load with respect to the center of mass of the helicopter and $\vec{\Omega} = p\vec{i}_B + q\vec{j}_B + r\vec{k}_B$ is its angular velocity. The absolute acceleration of the load is

$$\vec{a}_L = \vec{a}_{CG} + \ddot{R} + \dot{\vec{\Omega}}\times\vec{R} + 2\vec{\Omega}\times\dot{R} + \vec{\Omega}\times(\vec{\Omega}\times\vec{R}) \tag{7}$$

where $\vec{a}_{CG}$ is the acceleration of the center of mass of the helicopter. The weight vector is defined as

$$\vec{F}_G = mg(-\sin\varphi_F\vec{i}_{\mathrm{SP}} + \sin\varphi_F\cos\vartheta_F\vec{j}_{\mathrm{SP}} + \cos\varphi_F\cos\vartheta_F\vec{k}_{\mathrm{SP}}) \tag{8}$$

where φ_F and ϑ_F are the roll and pitch attitudes of the helicopter fuselage. The aerodynamic drag is

$$\vec{D}_L = \frac{1}{2}\rho|\vec{V}|\vec{V}C_DS \tag{9}$$

where C_D is the drag coefficient of a sphere ($C_D = 0.5$) and S is the sphere cross section.

By enforcing moment equilibrium about the suspension point, a system of three second-order differential equations is obtained here in matrix form:

$$\vec{R}_L\times(m\vec{a}_L + \vec{F}_G + \vec{D}_L) = 0 \tag{10}$$

Any two of these equations is sufficient to compute the solution. The force and the moment applied by the load to the helicopter are

$$\begin{aligned}\vec{F}_H &= m\vec{a}_L + \vec{F}_G + \vec{D}_L \\ \vec{M}_H &= \vec{R}_L \times \vec{F}_H\end{aligned} \tag{11}$$

This slung load model is in some way limited considering that the elasticity of the cable is neglected. This last point prevents the investigation of the vertical bounce phenomenon particularly significant for light helicopters. The following six-DOF rigid body model including cable elasticity effects overcomes these limitations.

External load as a rigid body

The second approach treats the external load as a rigid body. Nine full nonlinear equations evaluate linear velocities, angular rates, and attitude angles. Three additional equations account for the load center of mass position in an inertial reference frame. Twelve first-order nonlinear differential equations fully describe the load behavior. The cable is modeled as elastic but without mass and no aerodynamic effects. A small damping term is also added. Cable elasticity and damping values are taken from Refs. 11 and 13 for a conventional sling line configuration (see Fig. 1 from Ref. 11).

The six nonlinear first-order differential equations describing rigid body motion are the following:

$$\begin{aligned}\dot{u}_L &= X_L/m_L - w_L q_L + v_L r_L - g\sin(\theta_L) \\ \dot{v}_L &= Y_L/m_L + w_L p_L - u_L r_L + g\sin(\varphi_L)\cos(\theta_L) \\ \dot{w}_L &= Z_L/m_L + u_L q_L - v_L p_L + g\cos(\varphi_L)\cos(\theta_L) \\ \dot{p}_L &= L_L/Jy_L - p_L r_L(Jx_L - Jz_L)/Jy_L \\ \dot{r}_L &= N_L/Jz_L - p_L q_L(Jy_L - Jx_L)/Jz_L\end{aligned} \tag{12}$$

The system is derived for the case in which principal moments of inertia of the load are known. Three kinematic equations are added to account for the attitude angles:

$$\begin{aligned}\dot{\varphi}_L &= p_L + q_L\sin(\varphi_L)\tan(\theta_L) + r_L\cos(\varphi_L)\tan(\theta_L) \\ \dot{\theta}_L &= q_L\cos(\varphi_L) - r_L\sin(\varphi_L) \\ \dot{\psi}_L &= q_L\sin(\varphi_L)/\cos(\theta_L) + r_L\cos(\varphi_L)/\cos(\theta_L)\end{aligned} \tag{13}$$

Finally, three further equations account for load center of mass position in an inertial frame. These are, in matrix form,

$$[V_{\mathrm{LE}}] = [\dot{x}_{\mathrm{LE}}, \dot{y}_{\mathrm{LE}}, \dot{z}_{\mathrm{LE}}]^T = \left[L_{\mathrm{BE}_L}\right][u_{\mathrm{LB}}, v_{\mathrm{LB}}, w_{\mathrm{LB}}]^T \tag{14}$$

In the previous system of equations, X_L, Y_L, Z_L are the total forces and L_L, M_L, N_L the total moments acting on the load. Defined as vectors,

$$\begin{aligned}\vec{X}_L &= \vec{F}_A + \vec{F}_C \\ \vec{M}_L &= \vec{M}_A + \vec{R}_{\mathrm{LS}} \times \vec{F}_C\end{aligned} \tag{15}$$

where $\vec{F}_A$ and $\vec{F}_C$ are, respectively, the total aerodynamic forces and the cable forces along each of the axes, $\vec{M}_A$ is the aerodynamic moment and $\vec{R}_{\mathrm{LS}}$ is the position of the suspension point on the load with respect to the load center of mass defined as

$$\vec{R}_{\mathrm{LS}} = x_{\mathrm{LS}}\vec{i}_L + y_{\mathrm{LS}}\vec{j}_L + z_{\mathrm{LS}}\vec{k}_L \tag{16}$$

The elastic force along the cable $\vec{F}_{C_{\mathrm{el}}}$ is obtained as follows:

$$\vec{F}_{C_{\mathrm{el}}} = K\Delta\vec{L} \tag{17}$$

where K is the elastic constant of the cable and $\Delta\vec{L}$ is its elongation. Elongation is obtained by differencing the cable effective length $\vec{L}_{\mathrm{eff}}$ and the nominal cable length $\vec{L}$:

$$\Delta\vec{L} = \vec{L}_{\mathrm{eff}} - \vec{L} \tag{18}$$

where $\vec{L}_{\mathrm{eff}}$ is the difference of the position vector of the suspension point $\vec{X}_{\mathrm{HE}}$ and the position vector of the load center of mass $\vec{X}_{\mathrm{LE}}$ expressed in an inertial frame:

$$\vec{L}_{\mathrm{eff}} = \vec{X}_{\mathrm{HE}} - \vec{X}_{\mathrm{LE}} \tag{19}$$

The force due to the cable damping is obtained in a similar way:

$$\vec{F}_{C_\zeta} = \zeta\Delta\dot{\vec{L}} \tag{20}$$

where ζ is the cable damping coefficient and $\Delta\dot{\vec{L}}$ is the difference of the velocity vector of the suspension point $\vec{V}_{\mathrm{HE}}$ and the velocity vector of the load center of mass $\vec{V}_{\mathrm{LE}}$ expressed in an inertial frame:

$$\Delta\dot{\vec{L}} = \vec{V}_{\mathrm{HE}} - \vec{V}_{\mathrm{LE}} \tag{21}$$

A cable applies a force only if stretched. If the instantaneous cable length is below the nominal length, the cable does not apply any force on the helicopter, thus the total forces and moments applied by the load to the helicopter are

$$\begin{aligned}\Delta\vec{L} > 0 \quad &\rightarrow \quad \begin{cases}\vec{F}_H = \vec{F}_{C_{\mathrm{el}}} + \vec{F}_{C_\zeta} \\ \vec{M}_H = \vec{R}_H \times \vec{F}_H\end{cases} \\ \Delta\vec{L} \le 0 \quad &\rightarrow \quad \begin{cases}\vec{F}_H = 0 \\ \vec{M}_H = 0\end{cases}\end{aligned} \tag{22}$$

The great advantage of the rigid body formulation is that it takes aerodynamic effects and inertial properties of the load into account. The main disadvantage is the increased dimension of the system of differential equations needed to describe the system. In the present work, for comparison purposes with the pendulum model, the load is modeled as a sphere. As in the previous case, only isotropic drag is applied to the load. Inertial properties of the body are

$$J_{x_L} = J_{y_L} = J_{z_L} = \frac{2}{5}m_L r_L^2 \tag{23}$$

where r_L is the radius of the sphere. As in the previous case, aerodynamic forces and moments acting on the load reduce to

$$\begin{aligned}\vec{F}_A &= \vec{D}_L = \frac{1}{2}\rho|\vec{V}|\vec{V}C_D S \\ \vec{M}_A &= 0\end{aligned} \tag{24}$$

Main rotor wake model

The helicopter wake effect on the load is accounted for by a simple imposed wake model derived from Refs. 19 and 25. Using momentum theory, it is possible to evaluate the induced velocity at the rotor station in hover as follows:

$$v_{i_{\mathrm{Hover}}} = \sqrt{\frac{(m_H + m_L)\,g}{2\rho\pi R_{\mathrm{MR}}^2}} \tag{25}$$

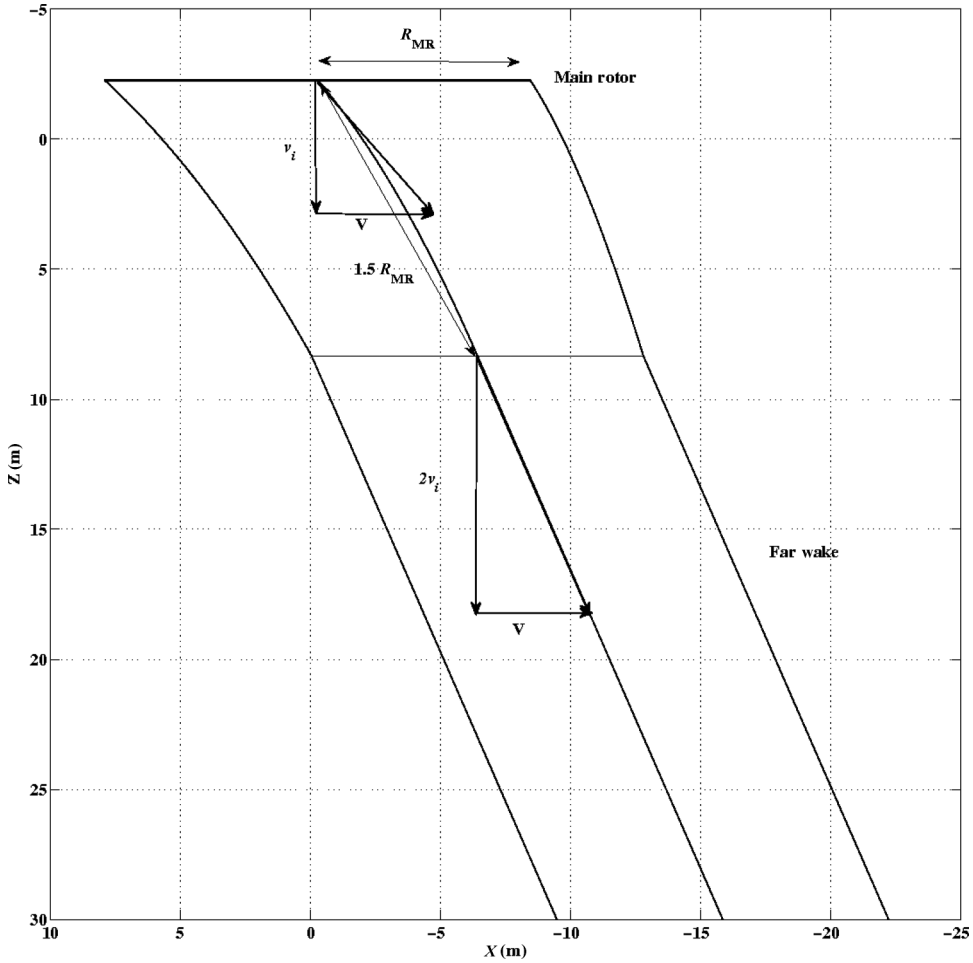

Fig. 2. Wake shape (20 kt).

It is possible to extend the induced velocity formulation to advancing flight (Refs. 26–28):

$$v_i = \sqrt{-\frac{V^2}{2} + \sqrt{\left[\frac{V^2}{2}\right]^2 + v_{i_{\text{Hover}}}^4}} \tag{26}$$

The induced velocity represents the vertical component of the rotor inflow, evaluated at the main rotor station. It is possible to define the wake skew angle as

$$\chi_{w_{\text{MR}}} = \arctan\left(\frac{v_i}{V}\right) \tag{27}$$

From momentum theory, it is known that the flow accelerates from v_i at the rotor to $2v_i$ at infinity. The skew angle will increase up to

$$\chi_{w_{\text{FW}}} = \arctan\left(\frac{2v_i}{V}\right) \tag{28}$$

For practical purposes, it is possible to assume that the wake is fully developed at a distance of 1.5 main rotor radii (Ref. 26).

Assuming a linear induced velocity increase from the rotor down to the far wake, a linear increase of the tangent of the χ_w angle is also obtained. The expression of the tangent is

$$\tan\chi_w = \dot{z} = ax + b \tag{29}$$

Since the tangent of the χ_w angle is the derivative of the wake center line, integration of its expression leads to the wake center line equation from the rotor to the beginning of the far wake:

$$z = \frac{1}{2}ax^2 + bx + c \tag{30}$$

Knowing that at the rotor hub station ($x = x_{\text{MR}}$; $z = z_{\text{MR}}$), with respect to the helicopter body frame,

$$\dot{z} = -\frac{v_i}{V} \tag{31}$$

and that at the beginning of the far wake

$$x^2 + z^2 = (1.5R_{\text{MR}})^2$$
$$\dot{z} = -\frac{2v_i}{V} \tag{32}$$

It is then possible to evaluate the position of the beginning of the far wake and the a, b, c coefficients, thus obtaining the expression of the wake centerline. The wake is then shaped around its centerline to evaluate its boundaries.

The main rotor generates a wake with a circular cross section. It is supposed here that the cross section maintains its shape down to the far wake, only decreasing its diameter. Momentum theory states that the mass flow is constant throughout each section of the wake. The continuity

Table 2. Load parameters in Refs. 11 and 12

Reference	Load Mass m_L (kg)	Load Drag Area C_{DS} (m^2)	Cable Length L (m)	Suspension Point Position versus CG		
				X (m)	Y (m)	Z (m)
11	1767	0.5	5.74	0.29	0	1.31
12	1000	0.5	5	0.2	0	1.25

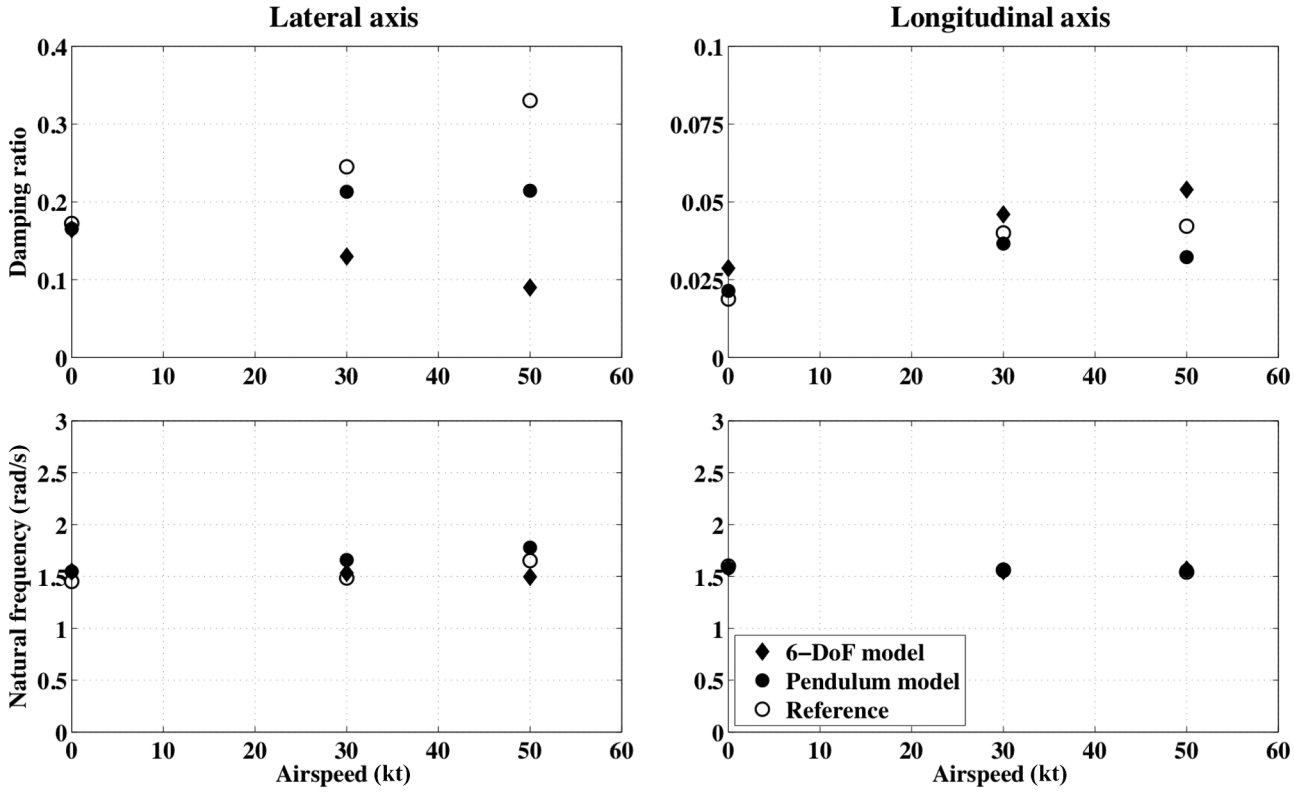

Fig. 3. Load pendulum roots comparison: Data from Ref. 12.

equation is only dependent on flow velocity and tube section. For two general sections, it is possible to write

$$\pi R^2{}_1 |V_1| = \pi R^2{}_2 |V_2| \rightarrow R_2 = R_1 \sqrt{\frac{|V_1|}{|V_2|}} \tag{33}$$

In the case where the first station is at the main rotor while the second is a generic wake section, it is possible to write

$$\begin{aligned} \pi R^2{}_{\mathrm{MR}} \sqrt{V^2 + v_i^2} &= \pi R^2{}_W \sqrt{V^2 + v_W^2} \\ R_W &= R_{\mathrm{MR}} \sqrt{\frac{\sqrt{V^2 + v_i^2}}{\sqrt{V^2 + v_W^2}}} \end{aligned} \tag{34}$$

where, given the linear approximation of the inflow increase between the rotor and the far wake,

$$\begin{aligned} v_W = v_i + \frac{v_i}{z_{\mathrm{FW}}} z_L \rightarrow z_{\mathrm{MR}} < z_L < z_{\mathrm{FW}} \\ v_W = 2v_i \rightarrow z_L \geq z_{\mathrm{FW}} \end{aligned} \tag{35}$$

Now that both the centerline and the radius of the wake are known, it is possible to compare the load position with respect to the wake. The load is considered inside the wake if the following inequality is satisfied:

$$\left(\frac{x_L - x_w}{R_w}\right)^2 + \left(\frac{y_L - y_w}{R_w}\right)^2 < 1 \tag{36}$$

In this case, the load velocity has to be augmented as follows:

$$\vec{V}_L = \vec{V}_L + \Delta\vec{V}_L \rightarrow \Delta\vec{V}_L = \begin{bmatrix} 0 \\ 0 \\ v_W \end{bmatrix} \tag{37}$$

In this work, as in Ref. 19, the wake only adds a vertical component to the load velocity. Moreover, the velocity distribution is supposed to be uniform at any given wake station. In contrast, Ref. 25 uses a more complex approach where the velocity distribution is a function of distance from the wake centerline. Figure 2 shows an example of the wake shape.

Solution Technique

To account for load effects, helicopter equations have to be modified. In particular, the differences between the equilibrium forces and moments and the actual forces and moments applied to the helicopter by the suspended load must be added to the vehicle dynamics. The first six

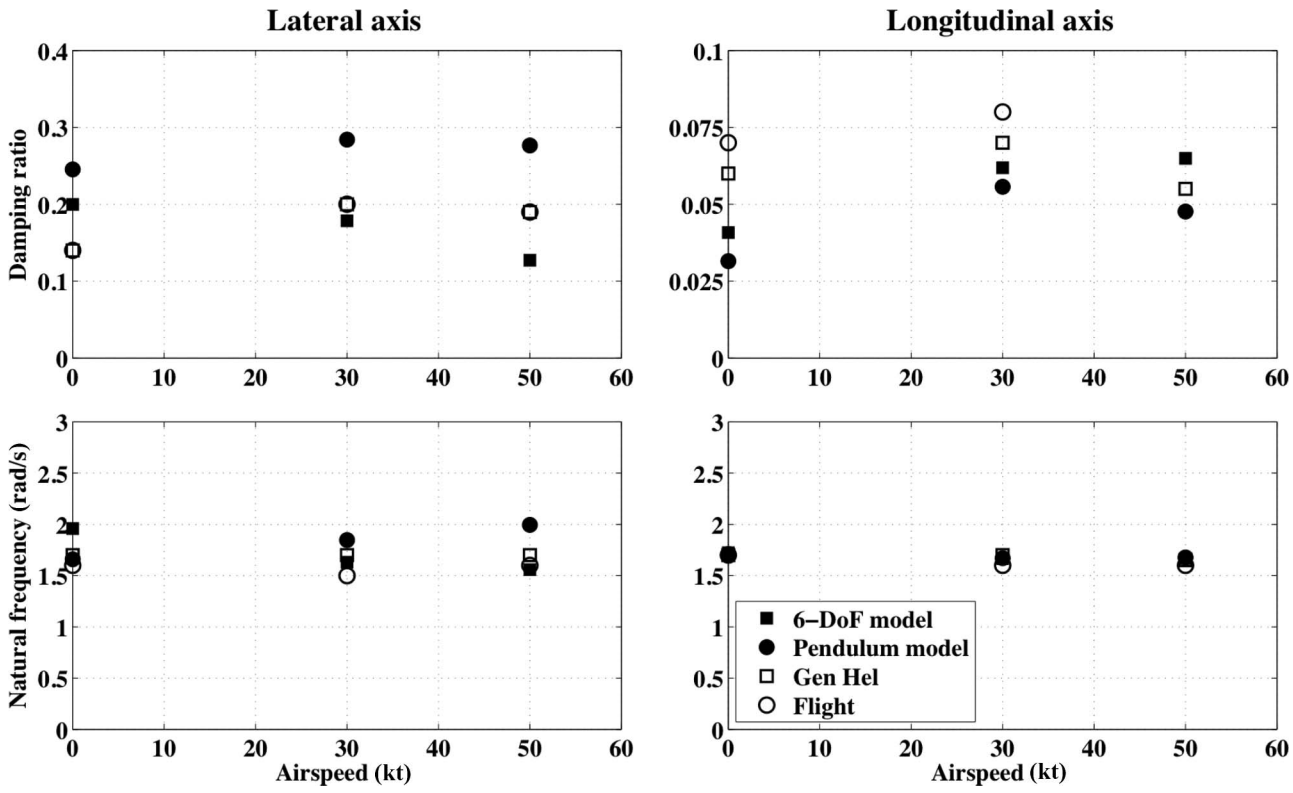

Fig. 4. Load pendulum roots comparison: Data from Ref. 11.

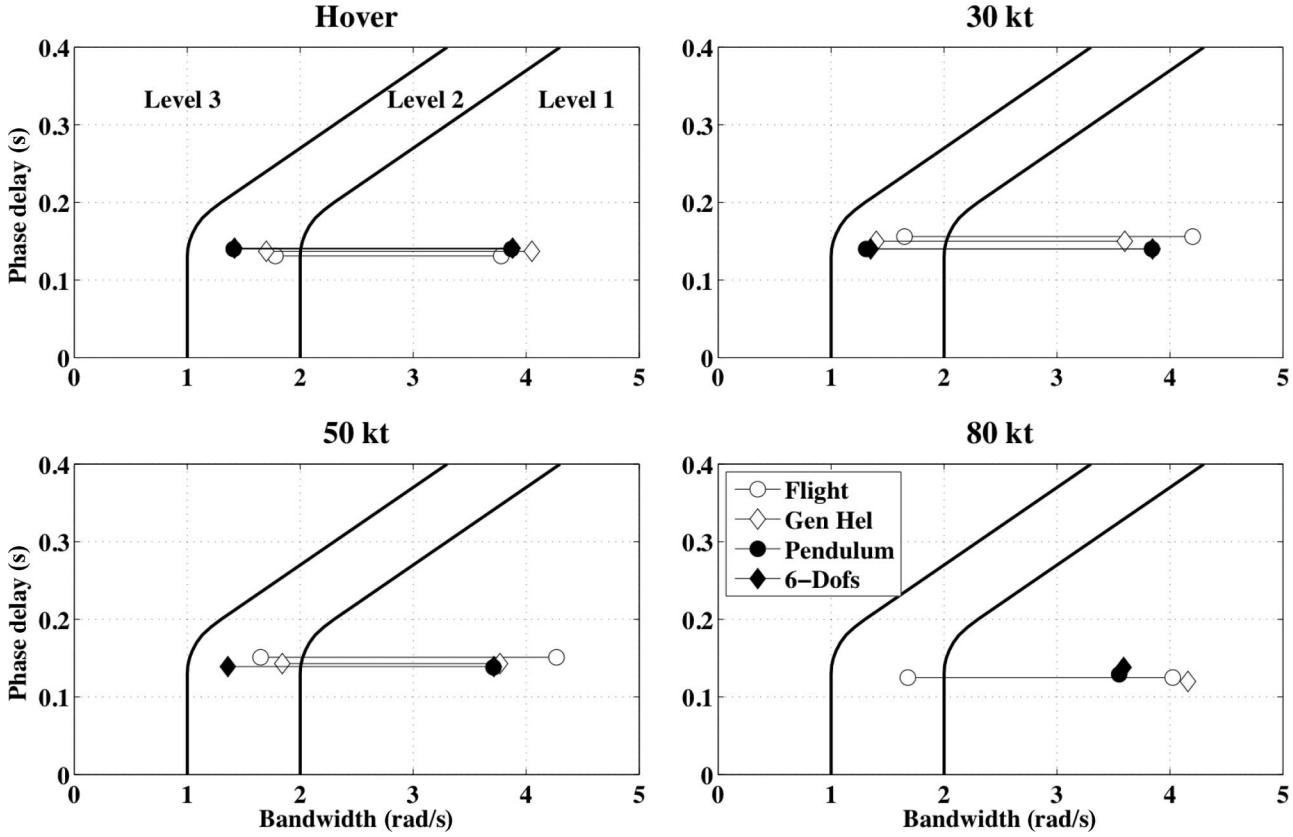

Fig. 5. Phase delay versus bandwidth: Lateral response (data from Ref. 11).

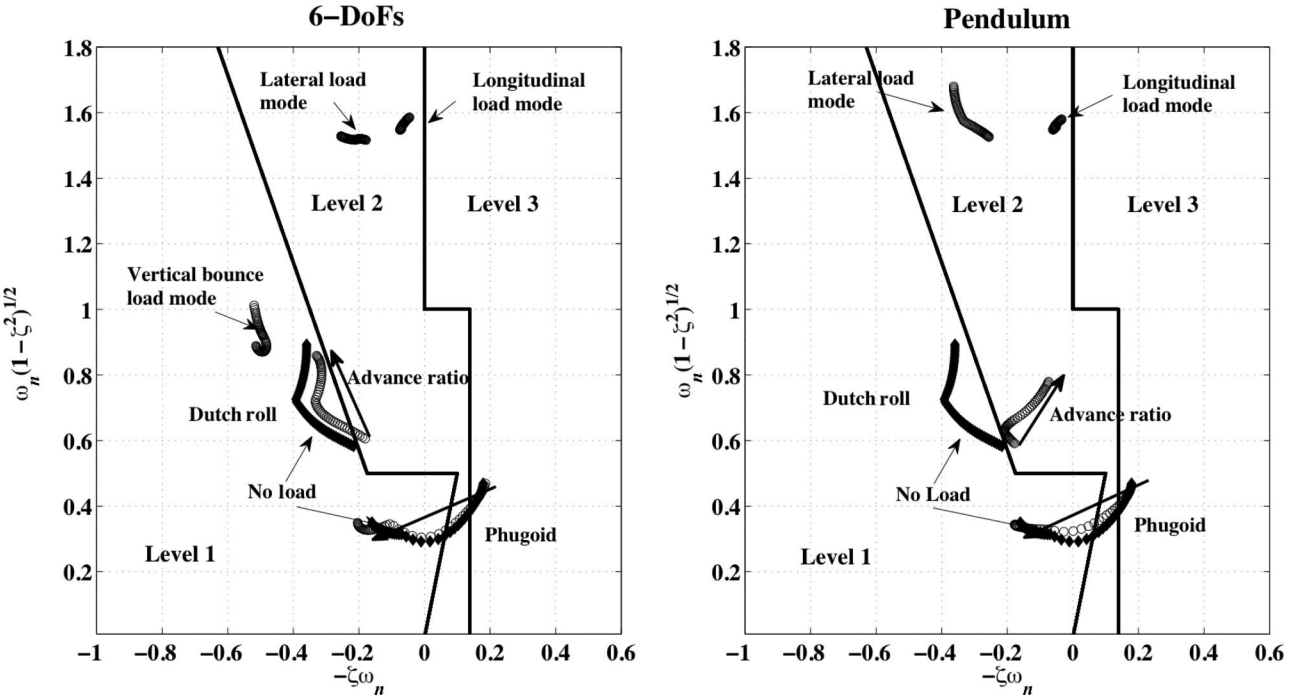

Fig. 6. Helicopter and load roots: Advance ratio variation $\mu = 0$–0.125.

Table 3. Slung load parameters

Parameter	Value
Advance ratio	0–0.125
Load mass m_L (kg)	500–1000–1500
Load drag area C_{DS} (m^2)	0.5
Cable length L (m)	3–5–7
Suspension point position versus CG	
X(m)	0.2
Y(m)	0
Z (m)	1.25

helicopter equations are modified as follows:

$$\begin{cases} \dot{u} = \dfrac{\Delta X_H}{m_H} + \displaystyle\sum_{i=1}^{9} A_{1,i}x_i \\ \dot{v} = \dfrac{\Delta Y_H}{m_H} + \displaystyle\sum_{i=1}^{9} A_{2,i}x_i \\ \dot{w} = \dfrac{\Delta Z_H}{m_H} + \displaystyle\sum_{i=1}^{9} A_{3,i}x_i \end{cases} \quad \begin{cases} \dot{p} = L'_H + \displaystyle\sum_{i=1}^{9} A_{4,i}x_i \\ \dot{q} = \Delta M_H + \displaystyle\sum_{i=1}^{9} A_{5,i}x_i \\ \dot{r} = N'_H + \displaystyle\sum_{i=1}^{9} A_{6,i}x_i \end{cases} \tag{38}$$

where

$$L'_H = \frac{\Delta L_H + \dfrac{J_{xz_H}}{J_{x_H}}\Delta N_H}{1 - \dfrac{J_{xz_H}^2}{J_{x_H}J_{z_H}}} \qquad N'_H = \frac{\Delta N_H + \dfrac{J_{xz_H}}{J_{z_H}}\Delta L_H}{1 - \dfrac{J_{xz_H}^2}{J_{x_H}J_{z_H}}} \tag{39}$$

where ΔL_H, ΔM_H, and ΔN_H are already normalized with their respective moments of inertia J_{x_H},J_{y_H}, and J_{z_H}. It is now possible to linearize the full system of differential equations composed by the helicopter equations (12 equations) and the load equations (either four equations for the pendulum model or 12 equations for the six-DOF model). Linearization

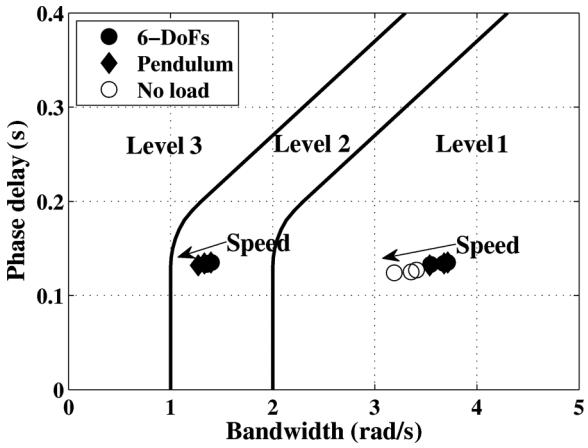

Fig. 7. Helicopter lateral response bandwidth and phase delay: Advance ratio variation $\mu = 0$–0.125.

is performed through the residues method. Starting from a trimmed condition, the states, the controls, and the derivative vector are iteratively perturbed. It is then possible to reconstruct a linear system of differential equations in the following form:

$$[E]\{d\dot{x}\} + [A_1]\{dx\} + [B_1]\{du\} = 0 \tag{40}$$

where $[E]$, $[A1]$, and $[B1]$ matrices are built as follows:

$$[A_1] = \begin{bmatrix} \dfrac{f_{1,1} - f_{0,1}}{\Delta x} & \cdots & \dfrac{f_{n,1} - f_{0,1}}{\Delta x} \\ \vdots & \ddots & \vdots \\ \dfrac{f_{1,n} - f_{0,n}}{\Delta x} & \cdots & \dfrac{f_{n,n} - f_{0,n}}{\Delta x} \end{bmatrix} \tag{41}$$

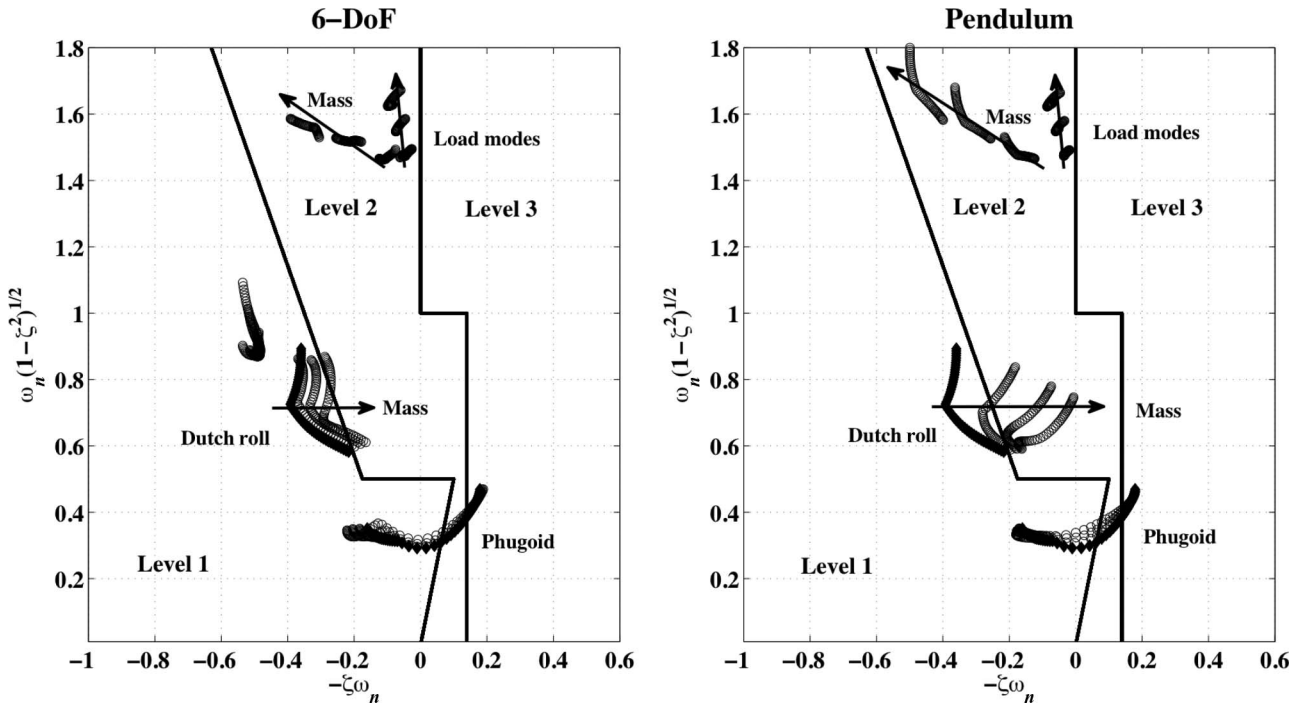

Fig. 8. Helicopter and load roots: Mass variation m_L = 500–100–1500 kg.

where

$$f = f(\dot{x}, x, u) \tag{42}$$

is the residual of the single differential equation. The impact of the increment Δx in the range $10^{-5} - 10^{-2}$ was found to be negligible in the present model formulation. Hence, it is possible to derive a state space system:

$$\begin{aligned} \{d\dot{x}\} &= [E]^{-1}[A_1]\{dx\} - [E]^{-1}[B_1]\{du\} \\ \{d\dot{x}\} &= [A]\{dx\} + [B]\{du\} \end{aligned} \tag{43}$$

The resulting formulation is used to assess the dynamic stability of the system by modal response analysis.

Results

Model validation

Longitudinal and lateral pendulum modes are the dynamics that mostly affect the helicopter motion in the frequency domain of interest for flight and handling qualities assessment (Ref. 13). To validate the pendulum model presented in this work, the results are compared with those available from Refs. 11 and 12. Natural frequency and damping of pendulum modes are evaluated for the load characteristics listed in Table 2. Reference 11 presents the results of simulations and flight tests, whereas the results of Ref. 12 are derived from simulations only.

Figure 3 compares results of the present analysis with data presented in Ref. 12. Both pendulum and six-DOF models match closely the natural frequency of the load modes. The damping ratio is also reproduced quite accurately for the longitudinal mode, whereas small differences are visible for the lateral mode at higher airspeeds.

Figure 4 compares current work with the results presented in Ref. 11. Again the pendulum and six-DOF models match the natural frequencies of the load modes. The damping ratio is matched accurately for both longitudinal and lateral modes.

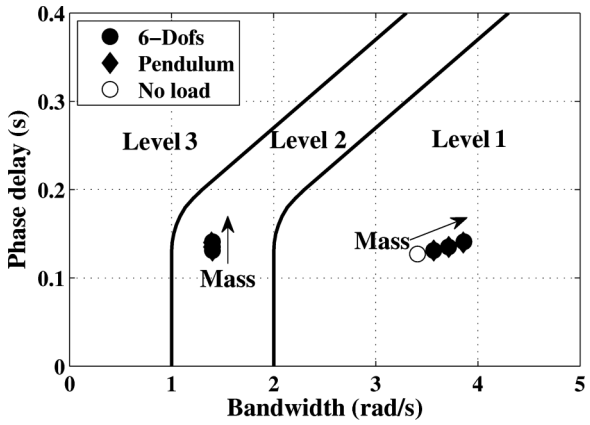

Fig. 9. Helicopter lateral response bandwidth and phase delay: Mass variation m_L = 500–100–1500 kg.

In Ref. 11, the response of the helicopter to command input is also available. Lateral response is the most affected by the presence of the slung load because the inertia around the roll axis J_X is smaller than the inertia of the other axes J_Y and J_Z. Thus the acceleration due to the same perturbation is larger (Ref. 11). It is then particularly interesting to compare the changes in bandwidth and phase delay of the roll response to a lateral cyclic command and to assess the effect on handling qualities. In the ADS-33 specifications (Ref. 20), the bandwidth and the phase delay are defined as

$$\begin{aligned} \omega_{BW} &= \min\{\omega_{6\text{db}}, \omega_{135}\} \\ \tau_{PD} &= -\frac{1}{2}\left(\frac{d\varphi}{d\omega}\right)_{\varphi=180} \end{aligned} \tag{44}$$

Figure 5 displays the results of the current analysis and those available from Ref. 11. The main effect of the suspended load is a drop of the phase

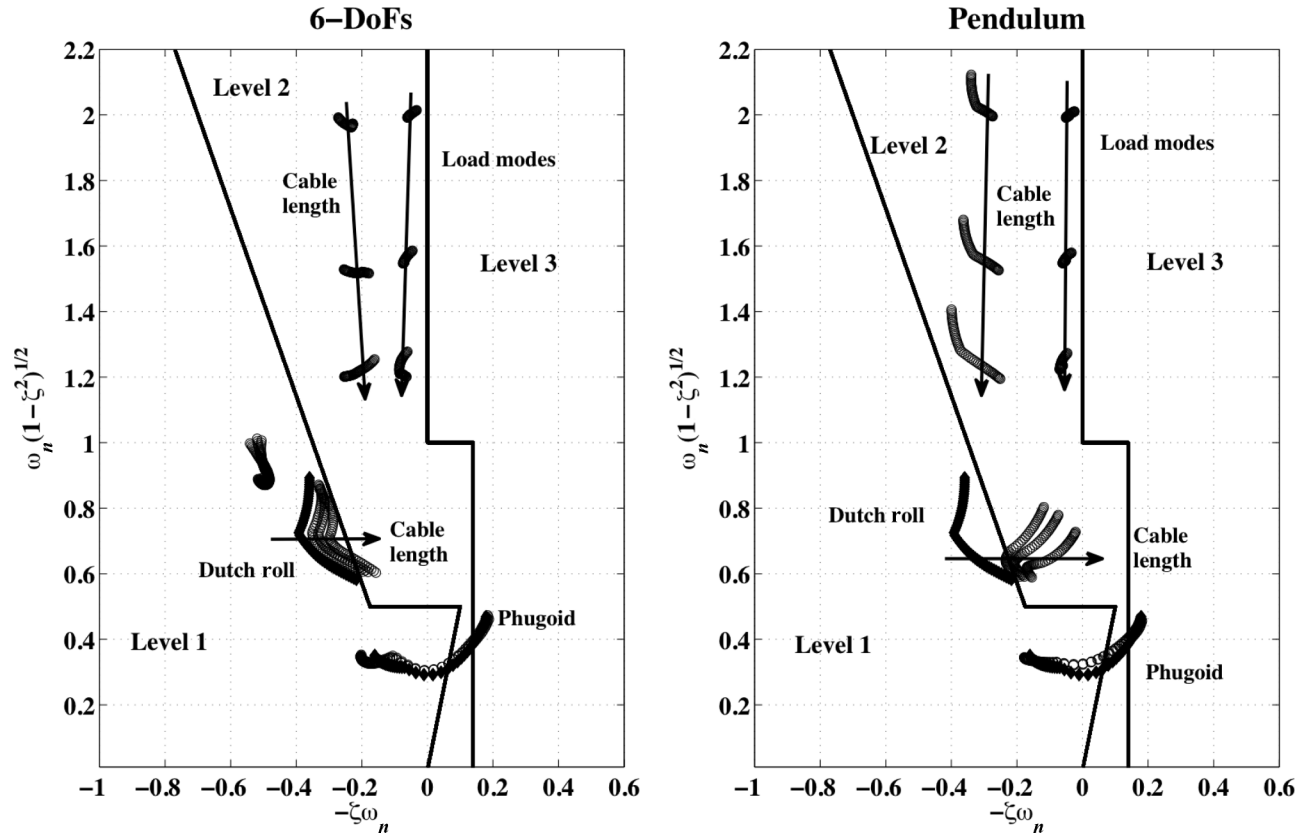

Fig. 10. Helicopter and load roots: Cable length variation L = 3–5–7 m.

at low frequency which causes a premature crossing of the $\varphi = -135^\circ$ phase limit and a marked reduction of bandwidth. The pendulum and the six-DOF models match well both the simulation and the flight-test results of Ref. 11 with very good prediction of the phase delay and only minor differences in the prediction of the bandwidth. The current model is unable to detect the bandwidth drop only in the 80-kt case where the Ref. 11 simulation is also unable to do so. The simplified helicopter model coupled with both the pendulum and the six-DOF load models is able to describe the slung load effect on the helicopter dynamics correctly, at least for moderate advance ratios.

Modal and frequency domain analysis

The analysis provides a preliminary assessment of coupled system dynamic stability trends with an advance ratio. Pendulum and six-DOF models are compared. The helicopter modal response and the roll response to lateral cyclic are shown for each test case. Every plot shows the helicopter modes without the suspended load for comparison purposes and includes handling qualities boundaries as addressed in Ref. 20.

The helicopter reference conditions are listed in Table 1, and the slung load characteristics are listed in Table 3.

Figure 6 shows the effect of increasing advance ratio from 0.0 to 0.125 on the helicopter and on the modal response of the suspended load. The black solid dots represent the helicopter phugoid and Dutch roll without the suspended load, whereas the empty dots represent the loaded helicopter modes and the slung load modes. As already discussed, the main effect of the slung load is on the lateral axis. The phugoid mode is almost unaffected, and both pendulum and six-DOF model trends with the advance ratio closely match those of the unloaded helicopter. The effect of the slung load on the Dutch roll is more relevant and leads to a degradation of the handling qualities. This is particularly true for the pendulum model where damping steadily decreases with the advance ratio. The six-DOF model exhibits more stable behavior.

Some differences can be seen in the load modes. In particular, the six-DOF model shows a third mode not present in the pendulum model. The eigenvector analysis shows it to be a damped vertical bounce involving load and helicopter vertical speed and position, but with very limited effect on other degrees of freedom. The vertical bounce is the result of the introduction of the cable elasticity.

Figure 7 shows the helicopter roll response to lateral cyclic in terms of bandwidth and phase delay. The solid dots are the pendulum and the six-DOF model results, whereas the unloaded helicopter is given by the empty dots. As discussed before, the main effect of the presence of the load is a premature crossing of the $\varphi = -135^\circ$ phase limit and a marked reduction of bandwidth. Increasing advance ratio further reduces bandwidth for both loaded and unloaded helicopter configurations.

Figure 8 shows the effect of increasing load mass. The phugoid mode is still almost unaffected, whereas the Dutch roll mode shows a marked degradation of damping with increasing load mass, particularly for the pendulum model. Lateral and longitudinal load modes experience a slight increase of their natural frequency with almost unchanged damping. The vertical bounce mode is affected in a very limited way.

Figure 9 shows that the main effect of the increase in load mass is a slight increase in phase delay. For clarity, only results for the hover case are presented.

Figure 10 shows the effect of the cable length. The most evident effect is the relevant reduction of the natural frequency of the load lateral and longitudinal modes. This effect is expected, and the natural frequency

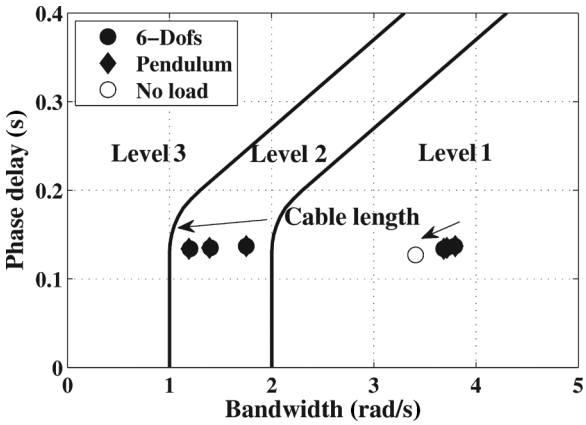

Fig. 11. Helicopter lateral response bandwidth and phase delay: Cable length variation $L = 3$–5–7 m.

closely matches the pendulum approximation:

$$\omega_p = \sqrt{\frac{g}{L}\left(1 - \frac{m_L}{m_H}\right)} \tag{45}$$

where g is the acceleration due to gravity, L the cable length, m_L the load mass, and m_H the helicopter mass (Ref. 13).

Again, the increase of the cable length has a marginal effect on the phugoid and tends to decrease the Dutch roll damping for both the pendulum and six-DOF models. Figure 11 shows a marked reduction of the bandwidth as cable length increases. For clarity, only results for the hover case are presented.

Conclusions

A simple state space helicopter model has been coupled with a pendulum and a six-DOF slung load model. The combined system modal response and the roll response to lateral cyclic input have been compared with available reference data, both from simulation and from flight-test experiments.

A parametric analysis of the effects of the slung load on helicopter dynamics and handling qualities has also been performed.

The results show that a preliminary assessment of flight and handling qualities for a helicopter with suspended load is possible using a very simple six-DOF helicopter state space model combined with either a pendulum or a six-DOF representation of the slung load. This is verified as long as the high-frequency rotor modes are far enough from the fuselage modes. In general, this is the case for light- and medium-sized helicopters.

As a final remark, the results of the present work suggest that preliminary assessment of the stability of a helicopter operating with a suspended load can be predicted quite accurately even with a simple modeling effort. This approach may be of interest for parametric design analysis and during the preliminary design phases when accurate simulation models are still unavailable. Further higher order analysis is obviously required to assess helicopter–load coupling in maneuvering flight and the impact of nonlinearities (rotor wake as an example).

Acknowledgments

This activity is part of a doctoral research program (Ph.D. in Aerospace Engineering at Politecnico di Torino) supported by the AgustaWestland Flight Mechanics Department.

References

[1]Manwaring, J. C., Conway, G. A., and Garrett, L. C., "Epidemiology and Prevention of Helicopter External Load Accidents," *Journal of Safety Research*, Vol. 29, (2), 1998, pp. 107–121.

[2]Lucassen, L. R., and Sterk, F. J., "Dynamic Stability Analysis of a Hovering Helicopter with a Sling Load," *Journal of American Helicopter Society*, Vol. 10, (2), 1965, pp. 6–12.

[3]Szustack, L. S., and Jenney, D., "Control of Large Crane Helicopters," *Journal of American Helicopter Society*, Vol. 16, (3), 1971, pp. 11–22.

[4]Dukes, T. A., "Maneuvering Heavy Sling load Near Hover, Part I: Damping the Pendulous Motion," *Journal of American Helicopter Society*, Vol. 18, (2), 1973, pp. 2–11.

[5]Smith, J. H., Allen, G. M., and Vensel, D., "Design, Fabrication, and Flight Test of the Active Arm External Load Stabilization System for Cargo Handling Helicopters," USAAMRDL Technical Report 73-73, 1973.

[6]Dukes, T. A., "Maneuvering Heavy Sling load Near Hover, Part II: Some Elementary Maneuvers," *Journal of American Helicopter Society*, Vol. 18, (3), 1973, pp. 17–22.

[7]Thanapalan, K., and Wong, T. M., "Modeling of a Helicopter with an Under-Slung Load System," 29th Chinese Control Conference Proceedings, Beijing, People's Republic of China, July 29–31, 2010.

[8]Nagabhushan, B., L., "Low-Speed Stability Characteristics of a Helicopter With a Sling Load," *Vertica*, Vol. 9, (4), 1985, pp. 345–361.

[9]Poli, C., and Cormack, D., "Dynamics of Slung Bodies Using a Single Point Suspension System," *Journal of Aircraft*, Vol. 12, (10), 1975, pp. 773–777.

[10]Cliff, E. M., and Bailey, D. B., "Dynamic Stability of a Translating Vehicle with a Simple Sling Load," *Journal of Aircraft*, Vol. 12, (10), 1975, pp. 849–856.

[11]Tyson, P. H., Cicolani, L. S., Tischler, M. B., Rosen, A., Levine, D., and Dearing, M., "Simulation Prediction and Flight Validation of UH-60A Black Hawk Slung-Load Characteristics," American Helicopter Society 55th Annual Forum Proceedings, Montreal, Canada, May 25–27, 1999.

[12]Fusato, D., Guglieri, G., and Celi, R., "Flight Dynamics of an Articulated Rotor Helicopter with an External Slung Load," *Journal of American Helicopter Society*, Vol. 46, (1), 2001, pp. 3–13.

[13]Cicolani, L. S., McCoy, A. H., Tischler, M. B., Tucker, G. E., Gatenio, P., and Marmar, D., "Flight-Time Identification of a UH-60A Helicopter and Slung Load," Proceedings of the NATO RTA Symposium on System Identification for Integrated Aircraft Development and Flight Testing, Madrid, Spain, May 5–7, 1998.

[14]Guglieri, G., and Quagliotti, F., "Effect of Main Rotor Configuration and Propulsion System Dynamics on Helicopter Handling Qualities," 21st ICAS Congress Proceedings, Melbourne, Australia, September 13–18, 1998.

[15]Cicolani, L., Cone, A., Theron, J. N., Robinson, D., Lusardi, J., Tischler, M. B., Rosen A., and Raz R., "Flight Test and Simulation of a Cargo Container Slung Load in Forward Flight," *Journal of American Helicopter Society*, **54**, 032006 (2009).

[16]Cicolani, L. S., da Silva, J. G. A., Duque, E. P. N., and Tischler, M. B. "Unsteady Aerodynamic Model of a Cargo Container for Slung-Load Simulation," *The Aeronautical Journal*, Vol. 108, (1085), 2004, pp. 357–368.

[17]Raz, R., Rosen, A., Carmeli, A., Lusardi, J., Cicolani, L., and Robinson, D., "Wind Tunnel and Flight Evaluation of Passive

Stabilization of a Cargo Slung Load," *Journal of American Helicopter Society*, **55**, 032001 (2010).

[18]Cicolani, L. S., and Kanning, G., "Equations of Motion of Slung-Load Systems, Including Multilift Systems," NASA TP 3280, 1992.

[19]Bisgaard, M., Bendtsen, J. D., and la Cour-Harbo, A. "Modeling of Generic Slung Load System," AIAA Modeling and Simulation Technologies Conference Proceedings, Keystone, CO, August 21–24, 2006.

[20]Anonymous, "Aeronautical Design Standard, Performance Specification, Handling Qualities Requirements for Military Rotorcraft," ADS-33E-PRF, U. S. Army Aviation and Missile Command, Aviation Engineering Directorate, Redstone Arsenal, AL, 2000.

[21]Hoh, R. H., Heffley, R. K., and Mitchell, D. G. "Development of Handling Qualities Criteria for Rotorcraft with Externally Slung Loads," NASA CR213488, 2006.

[22]Marguerettaz, P., and Guglieri, G., "Simulation of Helicopter Dynamics with External Suspended Load," 37th European Rotorcraft Forum Proceedings, Gallarate, Italy, September 13–15, 2011.

[23]Padfield, G. D., "On the Use of Approximate Models in Helicopter Flight Mechanics," *Vertica*, Vol. 5, 1981, pp. 243–259.

[24]Heffley, R. K., Jewell, W. F., Lehman, J. M., and Van Winkle, R. A., "A Compilation and Analysis of Helicopter Handling Qualities Data—Volume One: Data Compilation," NASA CR 3144, 1975.

[25]Tyson, P. H., "Simulation, Validation and Flight Prediction of UH-60A Black Hawk Helicopter Slung Load Characteristics," Master's Thesis, Naval Postgraduate School, Monterey, CA, 1999.

[26]Chen, R. T. N., "A Survey of Non-Uniform Inflow Models For Rotorcraft Flight Dynamics and Control Applications," NASA TM 102219, 1989.

[27]Bramwell, A. R. S., Done, G., and Balmford, D., *Helicopter Dynamics*, Butterworth-Heinemann, Oxford, UK, 2001.

[28]Johnson, W., *Helicopter Theory*, Dover, New York, NY, 1994.